RNA-binding proteins and heat-shock protein 90 are constituents of the cytoplasmic capping enzyme interactome

Received for publication, July 19, 2018, and in revised form, August 22, 2018 Published, Papers in Press, August 30, 2018, DOI 10.1074/jbc.RA118.004973

Jackson B. Trotman[‡§¶1,2], **Bernice A. Agana**[‡§‖1], **Andrew J. Giltmier**[‡¶3], **Vicki H. Wysocki**[‡‖], and **Daniel R. Schoenberg**[‡¶4]

From the [‡]*Center for RNA Biology,* [§]*Ohio State Biochemistry Program,* [¶]*Department of Biological Chemistry and Pharmacology, and* [‖]*Department of Chemistry and Biochemistry, Ohio State University, Columbus, Ohio 43210*

Edited by Ronald C. Wek

The N^7-methylguanosine cap is added in the nucleus early in gene transcription and is a defining feature of eukaryotic mRNAs. Mammalian cells also possess cytoplasmic machinery for restoring the cap at uncapped or partially degraded RNA 5′ ends. Central to both pathways is capping enzyme (CE) (RNA guanylyltransferase and 5′-phosphatase (RNGTT)), a bifunctional, nuclear and cytoplasmic enzyme. CE is recruited to the cytoplasmic capping complex by binding of a C-terminal proline-rich sequence to the third Src homology 3 (SH3) domain of NCK adapter protein 1 (NCK1). To gain broader insight into the cellular context of cytoplasmic recapping, here we identified the protein interactome of cytoplasmic CE in human U2OS cells through two complementary approaches: chemical cross-linking and recovery with cytoplasmic CE and protein screening with proximity-dependent biotin identification (BioID). This strategy unexpectedly identified 66 proteins, 52 of which are RNA-binding proteins. We found that CE interacts with several of these proteins independently of RNA, mediated by sequences within its N-terminal triphosphatase domain, and we present a model describing how CE-binding proteins may function in defining recapping targets. This analysis also revealed that CE is a client protein of heat shock protein 90 (HSP90). Nuclear and cytoplasmic CEs were exquisitely sensitive to inhibition of HSP90, with both forms declining significantly following treatment with each of several HSP90 inhibitors. Importantly, steady-state levels of capped mRNAs decreased in cells treated with the HSP90 inhibitor geldanamycin, raising the possibility that the cytotoxic effect of these drugs may partially be due to a general reduction in translatable mRNAs.

Cap homeostasis is a cyclical process of cytoplasmic decapping and recapping that impacts a subpopulation of the transcriptome. Previous work classified cytoplasmic capping targets into three groups based on conditions that impact the appearance of their uncapped forms (1). One group of mRNAs has a population of "natively uncapped" transcripts that become more susceptible to degradation by XRN1 when cytoplasmic capping is blocked. For another group, the "capping-inhibited" mRNAs, uncapped forms only appear when cytoplasmic capping is blocked. A third group, termed "common" mRNAs, overlaps with the natively uncapped pool but differs in that the representation of uncapped forms increases when cytoplasmic capping is blocked. We showed previously (2) that inhibition of cytoplasmic capping had no detectable impact on global poly(A) tail length. Uncapped forms of recapping targets accumulate in nontranslating mRNPs, and these have poly(A) tails similar in length to polysome-bound forms of the same mRNAs. As such, recapping is all that is needed to restore these mRNAs to the translating pool. Cytoplasmic recapping also appears to have a role in diversifying the transcriptome by acting on 5′-end–shortened products of post-transcriptional processing (3–7).

Enzymes capable of regenerating caps on cytoplasmic RNAs have been described in diverse eukaryotic systems (8, 9), but the most thoroughly characterized recapping system is that of mammalian cells. In mammals, CE[5] and RNA guanine-7 methyltransferase (RNMT) localize to both the nucleus and cytoplasm to participate in canonical cap synthesis and recapping, respectively (10–12). Cytoplasmic recapping is catalyzed by a complex of enzymes in the same pathway (*i.e.* a metabolon) that is capable of converting RNA with a 5′-monophosphate end to one with an m^7G cap. The core of this complex is NCK1, an adapter protein with three SH3 domains and a single SH2

This work was supported by National Institutes of Health Grant GM084177 (to D. R. S.) and funds from Ohio State University (to V. H. W.). The authors declare that they have no conflicts of interest with the contents of this article. The content is solely the responsibility of the authors and does not necessarily represent the official views of the National Institutes of Health, Pelotonia, or Ohio State University.

This article contains Table S1.

Mass spectrometry data have been deposited in the ProteomeXchange Consortium via the jPOST partner repository under the data set identifier PXD010368.

[1] Both authors contributed equally to this work.

[2] Supported by National Institutes of Health Training Grant GM08512 and a predoctoral fellowship from the Ohio State University Center for RNA Biology. Present address: Dept. of Pharmacology and Lineberger Comprehensive Cancer Center, University of North Carolina, Chapel Hill, NC 27599.

[3] Supported by a Pelotonia undergraduate fellowship from the Ohio State University Comprehensive Cancer Center.

[4] To whom correspondence should be addressed: Dept. of Biological Chemistry and Pharmacology, Ohio State University, Columbus, OH 43210. Tel.: 614-688-3012; Fax: 614-292-4118; E-mail: schoenberg.3@osu.edu.

[5] The abbreviations used are: CE, capping enzyme; RNMT, RNA guanine-7 methyltransferase; SH2 and SH3, Src homology 2 and 3, respectively; RAMAC, RNA guanine-7 methyltransferase–activating subunit; NES, nuclear export sequence; EGFP, enhanced GFP; PSM, peptide spectral match; RNGTT, RNA guanylyltransferase and 5′-phosphatase; ihRBP, integrated human RNA-binding proteome; GA, geldanamycin; DAPI, 4′,6-diamidino-2-phenylindole; WB, Western blotting; IF, immunofluorescence; BioID, biotin identification.

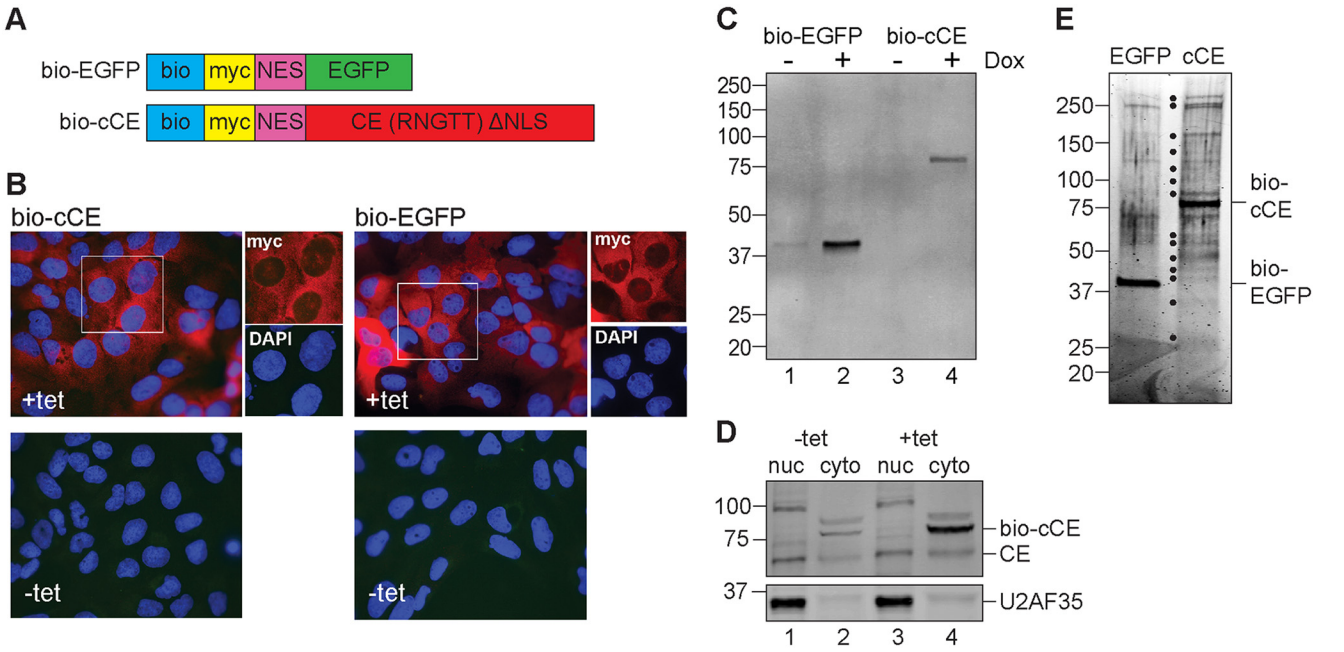

Figure 1. Development of stable cell lines for identifying the cytoplasmic CE interactome. *A*, *schematic* of bio-EGFP and bio-cCE constructs. Each of these proteins has an N-terminal tag that is biotinylated *in vivo*, a Myc epitope tag, and the HIV Rev NES. The nuclear localization sequence has also been removed from CE. *B*, immunofluorescence of U2OS-TR/bio-EGFP and U2OS-TR/bio-cCE stable cells grown in the presence (*top panels*) or absence of tetracycline (*bottom panels*) for 24 h. Cells were stained with mouse anti-Myc antibody and co-stained with DAPI and goat anti-mouse Alexa Fluor 594. The *images* to the *right* show the Myc (CE/EGFP) and DAPI channels, respectively, of the areas in *white boxes*. *C*, cytoplasmic extracts from uninduced and doxycycline-treated cells carrying bio-EGFP or bio-cCE transgenes were analyzed by Western blotting with Qdot 800 streptavidin conjugate. *D*, 10 μg of nuclear (*nuc*) and 30 μg of cytoplasmic (*cyto*) extracts of bio-cCE stable cells grown with or without tetracycline were analyzed by Western blotting with antibody against CE or U2AF35. Note that cytoplasmic extracts have a cross-reacting protein the same size as bio-cCE that is evident in the uninduced sample. *E*, proteins recovered on streptavidin beads with bio-EGFP or bio-cCE were separated on a 4–20% SDS-polyacrylamide gel and identified by Coomassie Blue staining. *Dots* indicate differentially recovered proteins.

domain. The kinase that generates a 5′-diphosphate recapping substrate binds to the second SH3 domain, and CE binds to the third SH3 domain. The latter interaction is mediated by a C-terminal proline-rich sequence of CE (13). The functional form of RNMT is a heterodimer with RNA guanine-7 methyltransferase–activating subunit (RAMAC, formerly called RAM (14)), and the RNMT:RAMAC dimer is recruited into the cytoplasmic capping complex by direct interaction with CE (12). A diagram of the cytoplasmic capping complex is shown in Fig. 5.

Immunofluorescence analysis of CE distribution (10) showed the expected nuclear staining and punctate focal staining of CE throughout the cytoplasm. Although it is tempting to think of the latter as focal sites of cytoplasmic recapping, we were unable to confirm this by co-staining for NCK1 due to the uniform distribution of that protein throughout the cytoplasm. This left open the question of whether the majority of cytoplasmic CE was in the recapping complex or if instead only a minor portion of the cytoplasmic protein participated in this process. This question gained significance with the recent identification of a role for cytoplasmic CE in regulating hedgehog signaling by antagonizing protein kinase A (8). To address this, we performed two complementary proteomics analyses of the cytoplasmic CE interactome using cells with stably integrated transgenes expressing cytoplasmically restricted forms of CE. The principal approach looked for proteins recovered with CE carrying an N-terminal sequence that is natively biotinylated *in vivo* (bio-cCE (13)). This was complemented by proximity-dependent biotinylation using protein with BirA* substituted for the biotinylation tag (BirA*-cCE (12)). The combined approaches identified 66 proteins as constituents of the cytoplasmic CE interactome. Strikingly, 52 of these have been characterized as RNA-binding proteins. This analysis also identified HSP90, and we show that nuclear and cytoplasmic CE are client proteins whose levels are dependent on HSP90 chaperone activity.

Results

Generation of cell lines for proteomics analysis

The initial approach to identifying the cytoplasmic CE interactome took advantage of a construct developed previously (13), termed bio-cCE, which expresses CE with an N-terminal sequence that is biotinylated *in vivo*. This protein is restricted to the cytoplasm by deletion of the KRKY nuclear localization signal and the addition of the HIV Rev nuclear export sequence (NES), modifications that were detailed (10). A plasmid expressing this cCE transgene was modified to introduce tetracycline operator elements and was stably transfected into tetracycline-inducible U2OS cells. To control for interacting proteins that may bind to the tags or interact nonspecifically, we also generated a cell line expressing a similarly tagged enhanced green fluorescence protein (bio-EGFP). These constructs included a Myc epitope tag (Fig. 1*A*). Immunofluorescence images in Fig. 1*B* show that each of these proteins was undetectable in the absence of tetracycline (−*tet*) and was only

Table 1

Cytoplasmic CE-interacting proteins identified by LC-MS/MS analysis

Listed are cytoplasmic CE-interacting proteins identified by MS analysis of samples recovered on streptavidin beads after formaldehyde cross-linking of cells expressing bio-cCE or bio-EGFP. The total number of PSMs from three independent experiments is listed. Details of each analysis are in Table S1. For each candidate interacting protein, a cCE enrichment index was calculated as the average of cCE PSMs divided by the average of negative control PSMs plus one. Column six lists proteins that were also identified by BioID, and column seven identifies proteins that appear in the integrated Human RNA-Binding Proteome (17). Proteins in boldface type were validated by Western blotting (Fig. 2). NA, not applicable.

Gene symbol	Gene name	Total PSMs		cCE enrichment index	BioID	ihRBP
		bio-cCE	bio-EGFP			
FASN	**Fatty acid synthase**	**76**	**9**	**6.33**	**Yes**	**Poly(A)**
KPNB1	Importin subunit β-1	17	0	5.67		Poly(A)
EEF2	**Elongation factor 2**	**47**	**6**	**5.22**	**Yes**	**Poly(A)**
CLTC	Clathrin heavy chain 1	40	5	5.00		Poly(A)
CCT5	T-complex protein 1 subunit ε	18	1	4.50		Non-poly(A)
CCT7	T-complex protein 1 subunit η	20	2	4.00		Non-poly(A)
CSE1L	**Exportin-2**	**12**	**0**	**4.00**		**Non-poly(A)**
CCT3	T-complex protein 1 subunit γ	24	3	4.00		Poly(A)
RUVBL2	**RuvB-like 2**	**11**	**0**	**3.67**		**Non-poly(A)**
CCT2	T-complex protein 1 subunit β	22	3	3.67		Non-poly(A)
TUBA3C	Tubulin α-3C/D chain	35	7	3.50		NA
TCP1	T-complex protein 1 subunit α	20	3	3.33		Poly(A)
TUBB6	Tubulin β-6 chain	46	11	3.29		NA
CCT8	T-complex protein 1 subunit θ	32	7	3.20	Yes	Non-poly(A)
TUBA1B	Tubulin α-1B chain	70	19	3.18	Yes	NA
TUBB	Tubulin β chain	123	37	3.08	Yes	Non-poly(A)
TUBB4B	Tubulin β-4B chain	109	33	3.03	Yes	NA
PSMD2	26S proteasome non-ATPase regulatory subunit 2	9	0	3.00		Non-poly(A)
CCT6A	T-complex protein 1 subunit ζ	14	2	2.80		Poly(A)
PHGDH	D-3-phosphoglycerate dehydrogenase	8	0	2.67		Non-poly(A)
FSCN1	Fascin	8	0	2.67		Poly(A)
TIMM50	Mitochondrial import inner membrane translocase subunit TIM50	8	0	2.67		NA
AHNAK	Neuroblast differentiation–associated protein AHNAK	16	3	2.67	Yes	Poly(A)
HSP90AB1	**Heat shock protein HSP 90-β**	**85**	**29**	**2.66**	**Yes**	**Poly(A)**
HSP90AA1	**Heat shock protein HSP 90-α**	**48**	**16**	**2.53**	**Yes**	**Poly(A)**
FKBP4	Peptidyl-prolyl *cis-trans*-isomerase FKBP4	10	1	2.50		Poly(A)
TLN1	Talin-1	10	1	2.50		Non-poly(A)
CCT4	T-complex protein 1 subunit δ	22	6	2.44		Poly(A)
EIF2S1	Eukaryotic translation initiation factor 2 subunit 1	12	2	2.40		Poly(A)
RNH1	Ribonuclease inhibitor	7	0	2.33		Non-poly(A)
MTHFD1	C-1-tetrahydrofolate synthase, cytoplasmic	9	1	2.25		Non-Poly(A)
PCBP2	Poly(rC)-binding protein 2	9	1	2.25		Poly(A)
HSPA1A	Heat shock 70-kDa protein 1A/1B	11	2	2.20		NA
STIP1	Stress-induced phosphoprotein 1	11	2	2.20		Poly(A)
FLNC	Filamin-C	24	8	2.18		NA
TUBA1C	Tubulin α-1C chain	16	5	2.00		Poly(A)
GAPDH	Glyceraldehyde-3-phosphate dehydrogenase	19	7	1.90		Poly(A)
PCBP1	Poly(rC)-binding protein 1	9	2	1.80		Poly(A)
ENO1	α-enolase	7	1	1.75	Yes	Poly(A)
KIF5B	Kinesin-1 heavy chain	5	0	1.67		Non-poly(A)
RUVBL1	**RuvB-like 1**	**5**	**0**	**1.67**		**Non-poly(A)**
FLNA	Filamin-A	46	25	1.64		Poly(A)
RAN	GTP-binding nuclear protein Ran	6	1	1.50		Poly(A)
PFN1	Profilin-1	6	1	1.50	Yes	Poly(A)
EIF5A	Eukaryotic translation initiation factor 5A-1	9	3	1.50		Poly(A)

observed in the cytoplasm of tetracycline-treated cells (+*tet*). Streptavidin Western blotting of cytoplasmic extracts confirmed that both proteins were biotinylated. This also showed a small amount of leaky expression of bio-EGFP and no evidence for leaky expression of bio-cCE (Fig. 1*C*). Western blotting of nuclear and cytoplasmic extracts with anti-CE antibody provided additional evidence showing that bio-cCE is restricted to the cytoplasm (Fig. 1*D*). Note that cytoplasmic extracts have a cross-reacting protein the same size as bio-cCE that makes the overall induction appear greater than it actually was.

Identification of cCE-interacting proteins

Stable cells were briefly cross-linked with formaldehyde before harvesting to preserve *in vivo* interactions of proteins with bio-EGFP and bio-cCE (16). As proof of principle, cytoplasmic proteins recovered on streptavidin paramagnetic beads were visualized by SDS-PAGE and Coomassie Blue staining (Fig. 1*E*). This provided evidence for the selective recovery of at least 14 proteins with bio-cCE that were not recovered with bio-EGFP. Several proteins were also identified in both samples, likely as contaminants that bound nonspecifically to the streptavidin beads or to the common N-terminal peptide tags.

This experiment was then repeated three times, with bead-bound proteins identified by LC coupled to tandem MS (LC-MS/MS) of tryptic peptides. The numbers of peptide spectral matches (PSMs) were tallied for each protein identified, and results are presented in Table 1. For each protein, a cCE enrichment index was calculated as the average number of PSMs for bio-cCE divided by the average number of PSMs for bio-EGFP plus one. The addition of one to the denominator was done to prevent division by zero and to de-emphasize proteins with fewer PSMs. As expected, PSMs for CE (RNGTT) were exclusive to the bio-cCE samples (Table S1). These data indicate that cytoplasmic CE interacts with many more proteins than previously thought. Forty-five proteins were identified as having a

cCE enrichment index of at least 1.5 (Table 1). Unexpectedly, this list did not include the two known cCE-interacting proteins NCK1 (13) and RNMT (12). The reason for this is unclear; however, we suspect that this may indicate that at any given time, only a minor portion of cytoplasmic CE associates with the previously described functional recapping complex (see "Discussion"). Likewise, no obvious candidate protein was identified that may harbor 5′-monophosphate kinase activity, although the possibility of uncharacterized kinase activity in the identified proteins cannot be ruled out.

The most striking observation is that 38 (84%) of the cytoplasmic CE interactors are classified as RNA-binding proteins in a recent comprehensive analysis of the human RNA-binding proteome (17) (Table 1). That study compiled an "integrated human RNA-binding proteome" (ihRBP) containing 978 known poly(A) RNA–binding proteins (18–20) and an additional 775 novel nonpoly(A) RNA–binding proteins. In our cytoplasmic CE interactome, 24 proteins are classified as poly(A) RNA–binding, and 14 proteins are nonpoly(A) RNA–binding. This list of proteins did not include proteins identified by Youn *et al.* (21) (mainly RNA polymerase II subunits, regulators of transcription elongation, and protein phosphatase 4 subunits) as CE-interacting proteins. That is not altogether surprising, because that study used total cell extracts, and CE is mostly a nuclear protein (see Fig. 1*D*; also see Fig. 1*D* in Otsuka *et al.* (10)).

BioID of the cytoplasmic CE interactome

In previous work (12), proximity-dependent biotinylation was used to obtain supporting evidence for the presence of cap methyltransferase (RNMT) in complex with cytoplasmic CE. The BirA*-cCE construct used in that study was modified to create a tetracycline-inducible transgene, which was stably transfected into U2OS-TR cells. As a specificity control, we also developed U2OS-TR cells with inducible BirA* fused only to the HIV Rev NES and the linker peptides present in BirA*-cCE. These were then used to generate orthogonal data to those obtained above with bio-cCE. The background of proteins detected with BirA* alone was higher than that obtained with bio-EGFP, perhaps as a result of nonspecific biotinylation by freely diffusing protein. When this was taken into account, BioID identified 32 proteins with a cCE enrichment index of at least 1.25 (Table S1), 11 of which were common to both proteomics analyses (Table 1). Of the 32 proteins identified by BioID, 23 (72%) were classified as RNA-binding in the ihRBP (17) (Table S1). Together, the combined approaches identified 66 CE-interacting proteins, 52 (79%) of which are represented in the integrated human RNA-binding proteome. Our reasoning for classifying all of these as cytoplasmic CE-interacting proteins is covered under "Discussion."

Validation and characterization of cytoplasmic CE protein interactions

To confirm these results, we selected six proteins representing a range of PSMs for further analysis by Western blotting. These included heat shock protein 90 (48 and 85 PSMs for the α and β isoforms, respectively) at the high end, RuvB-like AAA ATPase 1 (RUVBL1) at the low end (5 PSMs), and several

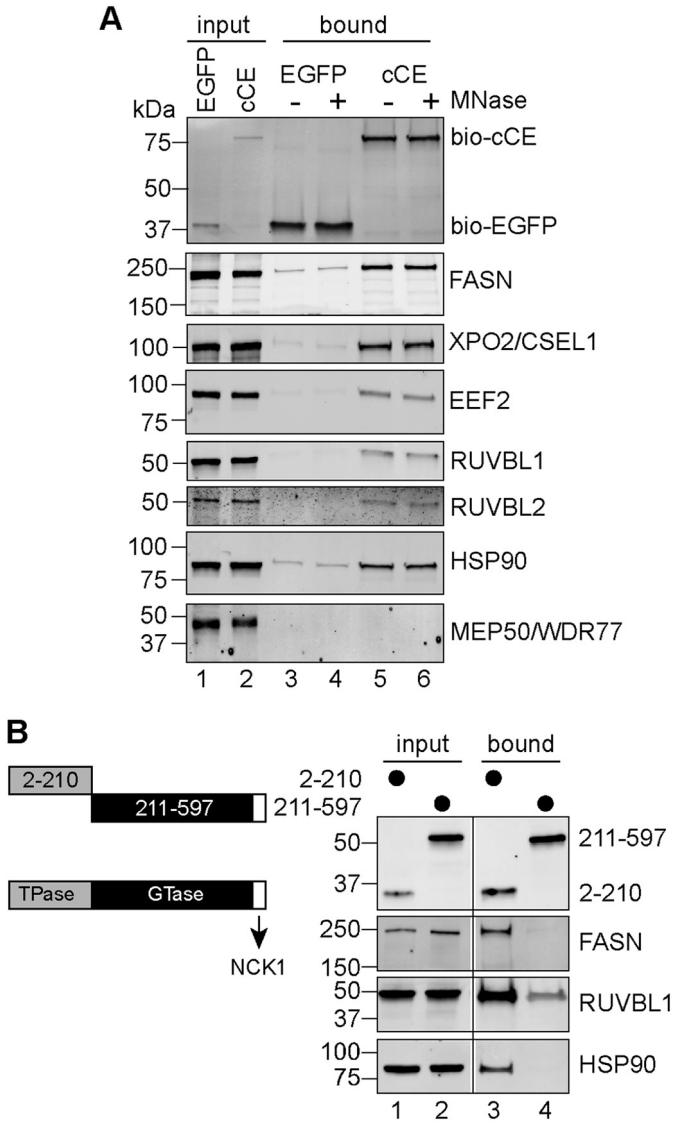

Figure 2. Validation of interactions with cytoplasmic CE. *A*, stably transfected U2OS-TR cells were induced as in Fig. 1 to express bio-EGFP or bio-cCE. Cytoplasmic extracts were pretreated with or without micrococcal nuclease before incubation with streptavidin beads. 1% of input and 50% of bead-bound material were analyzed by Western blot analysis using streptavidin-800 conjugate (*top*) and antibodies to FASN, XPO2/CSEL1, EEF2, RUVBL1, RUVBL2, HSP90, and MEP50/WDR77. *B*, the *left panel* shows the domain structure of CE and its derivatives with the C-terminal NCK1-binding site indicated. *TPase*, triphosphatase domain; *GTase*, guanylyltransferase domain. In the *right panel*, HEK293 cells were transiently transfected with plasmids expressing each of the indicated domains (bio-CE 2–210 (TPase domain) or bio-CE 211–597 (GTase domain)). Cells were processed and analyzed as in *A*. The CE domain constructs (*top*) were detected with an anti-Myc antibody, and co-recovered proteins were detected with antibodies to the indicated proteins. The gels used for these blots had an unrelated sample between lanes containing the input and bound fractions. The excised lanes are indicated by a *vertical line*.

in between: fatty acid synthase (FASN), exportin-2 (XPO2/CSE1L), translation elongation factor 2 (EEF2), and RuvB-like AAA ATPase 2 (RUVBL2) (Fig. 2*A*). As a negative control, we also probed the streptavidin-bound material with an antibody against methylosome protein 50 (MEP50/WDR77), which was not identified by our proteomics analysis. With the exception of MEP50, each of these proteins was selectively recovered with bio-cCE but not with bio-EGFP (compare *lanes 3* and *5*).

Although CE is not an RNA-binding protein, it was formally possible that these proteins were co-recovered as a consequence of mutual interactions with RNA molecules. To control for this, the same extracts were treated with micrococcal nuclease (13) before binding onto streptavidin beads (*lanes 4* and *6*). Nuclease digestion had no impact on the recovery of any of these proteins, thus ruling out mutual RNA binding as a factor in their appearance in the CE interactome.

CE has two catalytic domains, the triphosphatase domain spanning residues 1–210 and the guanylyltransferase domain spanning residues 211–597. We previously showed that a C-terminal proline-rich sequence is required for binding of CE to NCK1 and its recruitment into the cytoplasmic capping complex (13). To narrow down the interaction site on CE, the experiment in Fig. 2*A* was repeated using cells transfected with plasmids that separately express residues 2–210 and 211–597. FASN, RUVBL1, and HSP90 were each recovered with residues 2–210 (*i.e.* the N-terminal triphosphatase domain) but not with residues 211–596 (the C-terminal guanylyltransferase domain; Fig. 2*B*). Given their size (*e.g.* FASN is 2511 amino acids) and diverse nature, it is unlikely that CE-interacting proteins bind simultaneously to the N-terminal domain of CE. Instead, these data suggest that cytoplasmic CE has many interacting partners, with each protein representing a separate binding event.

Identification of CE as an HSP90 client protein

HSP90 is an ATP-dependent protein chaperone that helps fold and stabilize a select but diverse group of client proteins, including protein kinases, transcription factors, and disease-related factors such as p53 and Tau (22, 23). HSP90 functions as a chaperone constitutively, but expression of both the α and β isoforms increases in response to protein-denaturing stressors to help stabilize client proteins (24, 25). We were struck by the high PSMs for HSP90 (Table 1), and its parallel identification by BioID suggested that CE might be an HSP90 client protein.

Geldanamycin is a natural product that specifically inhibits HSP90 by binding to its unique ATP-binding site (26). Adding geldanamycin to the medium of cells expressing the bio-cCE transgene reduced the overall level of this protein to 32% of the DMSO-treated control (Fig. 3*A*). This experiment was repeated using nontransfected U2OS cells to determine whether geldanamycin had a similar impact on endogenous CE or if the observed loss in Fig. 3*A* resulted from interference with the induction process (Fig. 3*B*). Treating cells with geldanamycin resulted in a 50% loss of nuclear CE and 70% loss of cytoplasmic CE, thus confirming the identity of CE as an HSP90 client protein. In a separate experiment, the effect of geldanamycin inhibition was evident within 3 h of exposure (Fig. 3*C*), with nuclear CE reduced 80% and cytoplasmic CE reduced 60% after 24 h.

HSP90 inhibitors are in development as therapeutic agents for cancer and other diseases (26). We therefore looked at the impact of two additional HSP90 inhibitors with distinct modes of binding to the ATP-binding pocket: radicicol and AT13387 (onalespib), a second-generation HSP90 inhibitor that is currently in clinical trials. Nuclear and cytoplasmic CE declined by 30% following treatment with 1 μM radicicol, and nuclear CE continued to decline with increasing concentrations (Fig. 3*D*). Similar results were also observed for onalespib (Fig. 3*E*). With each of these inhibitors, the decline in nuclear CE was greater than that observed for cytoplasmic CE. Whereas the majority of HSP90 localizes to the cytoplasm, a small population has been reported to function in the nucleus as well (27, 28). Thus, the simultaneous loss of nuclear and cytoplasmic CE upon HSP90 inhibition could be due to redistribution of CE via nucleocytoplasmic shuttling or due to direct action of HSP90 on mature nuclear CE.

HSP90 inhibition is associated with decreased steady-state levels of capped mRNAs

CE loss results in apoptosis (29), and whereas capping is essential for cell growth and viability, to date, this process had not been examined for sensitivity to HSP90 inhibition. To address this, we examined the impact of geldanamycin treatment on steady-state levels of a number of mRNAs used in previous studies on cytoplasmic capping. In the experiment in Fig. 4*A*, cytoplasmic RNA recovered from control (DMSO) or geldanamycin (GA)-treated cells was spiked with internal controls of uncapped luciferase mRNA and capped mCherry mRNA. Relative levels of these mRNAs were then quantified by quantitative RT-PCR with results normalized to mCherry RNA. As expected, treating cells with geldanamycin had no impact on the relative amounts of the spike-in luciferase control. Geldanamycin also had no impact on the steady-state level of 18S rRNA, which is not a substrate of CE. However, steady-state levels of every mRNA examined declined following geldanamycin treatment. This included mRNAs that are cytoplasmic capping targets (*MAPK1*, *POLR2B*, *VDAC3*, and *ZNF207*) as well as mRNAs that are not targets of cytoplasmic recapping (*RPLP0* and *STRN4*).

Cells have a number of surveillance mechanisms for degrading uncapped or improperly capped mRNAs (30, 31), and capping is required for RNA polymerase II transcription elongation and nuclear RNA export (32). Thus, if nuclear capping was diminished in geldanamycin-treated cells, the surviving cytoplasmic mRNAs should still be capped despite their lower levels. eIF4E is highly selective for binding m^7G capped mRNAs (33), and Trotman *et al.* (12) used immobilized eIF4E to assay the cap status of mRNAs that survive inhibition of cytoplasmic cap methylation. eIF4E binds mRNAs with differing efficiency, and this was evident by differences in mRNA recovery in Fig. 4*B*. Uncapped luciferase mRNA and 18S rRNA were almost undetectable in the eIF4E-bound fraction. This contrasts with *STRN4*, which was bound just as efficiently as capped mCherry RNA. Importantly, there was no statistically significant difference in the recovery of capped mRNAs examined here from control or geldanamycin-treated cells. This finding indicates that the decline in each of these species following inhibition of HSP90 is due to a decrease in the steady-state level of capped forms of these mRNAs.

Discussion

The identification (10) of a cytoplasmic pool of CE led to the discovery of a cyclical process of cytoplasmic decapping and recapping termed cap homeostasis (1). Cap homeostasis maintains the stability and translation of a limited portion of the transcriptome and is facilitated by a complex of enzymes that

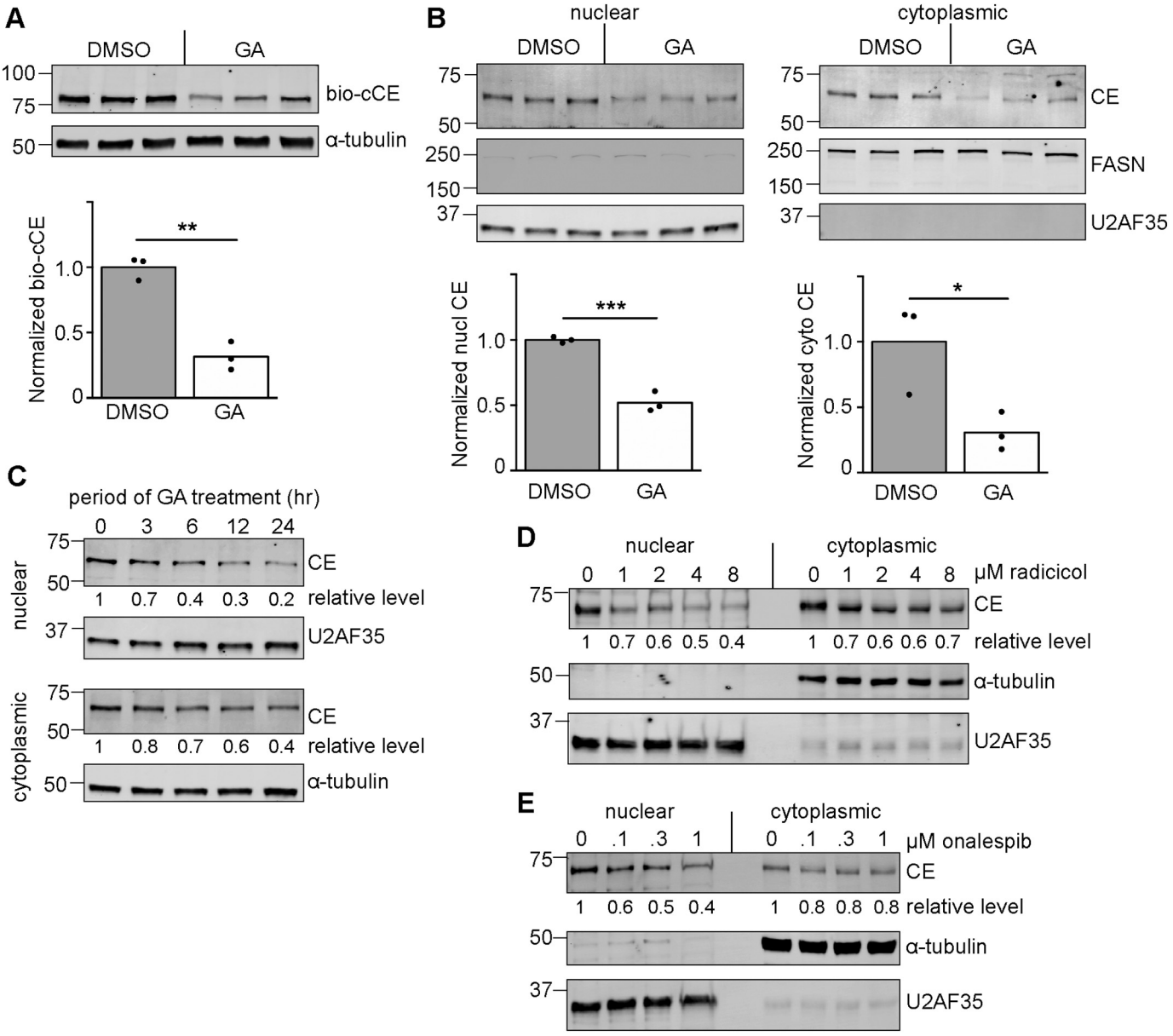

Figure 3. Impact of HSP90 inhibitors on nuclear and cytoplasmic CE. *A*, triplicate cultures of U2OS-TR/bio-cCE cells were induced with 0.2 μg/ml tetracycline and maintained in the presence of 0.2 μM GA or DMSO vehicle control for 24 h. Cytoplasmic extracts were analyzed by Western blotting with anti-Myc and anti-α-tubulin antibodies. Quantified, averaged Western blotting data (LI-COR) are shown graphically, with the *bar* representing the mean and each *dot* representing an individual replicate of the Myc signal normalized to α-tubulin. *B*, the experiment in *A* was repeated using cytoplasmic and nuclear extracts from uninduced U2OS-TR cells. Endogenous CE was detected by Western blotting with anti-CE antibody. For graphical analysis, nuclear CE was normalized to U2AF35, and cytoplasmic CE was normalized to FASN, and individual replicates are indicated as in *A* on each *bar graph*. *C*, U2OS-TR cells were treated with 0.2 μM GA for the indicated time before harvesting. Nuclear and cytoplasmic extracts were analyzed by Western blotting with antibodies to CE, U2AF35 (nuclear extracts), and α-tubulin (cytoplasmic extracts). *D* and *E*, U2OS-TR cells were grown for 24 h in the indicated concentration of radicicol (*D*) or onalespib (*E*). Nuclear and cytoplasmic extracts were analyzed as in *B* with normalized data shown *below* the CE Western blots. *, $p < 0.05$; **, $p < 0.01$; ***, $p < .001$ by unpaired two-tailed *t* test.

catalyze the sequential phosphorylation, guanylation, and cap methylation of decapped forms of these mRNAs.

Previous studies of CE-interacting proteins focused on the relationship of CE to transcription and nuclear pre-mRNA processing (see Ramanathan *et al.* (34) for a recent review). The current study used two complementary approaches to identify the cytoplasmic CE interactome. The first used a form of capping enzyme with a sequence tag that is biotinylated *in vivo* (bio-cCE (13)). This protein is restricted to the cytoplasm by deletion of the four-amino acid nuclear localization sequence and the addition of the HIV Rev nuclear export sequence. The addition of a Myc epitope tag facilitated detection by immunofluorescence and Western blotting (Fig. 1). Inducible transgenes expressing cytoplasmic CE or EGFP with similar modifications were stably transfected into tetracycline-inducible U2OS cells, and proteins recovered on streptavidin beads were identified by LC-MS/MS of tryptic fragments. These results were complemented by BioID using an inducible transgene (BirA*-cCE (12)) that differed from bio-cCE by substitution of BirA* for the biotinylation tag.

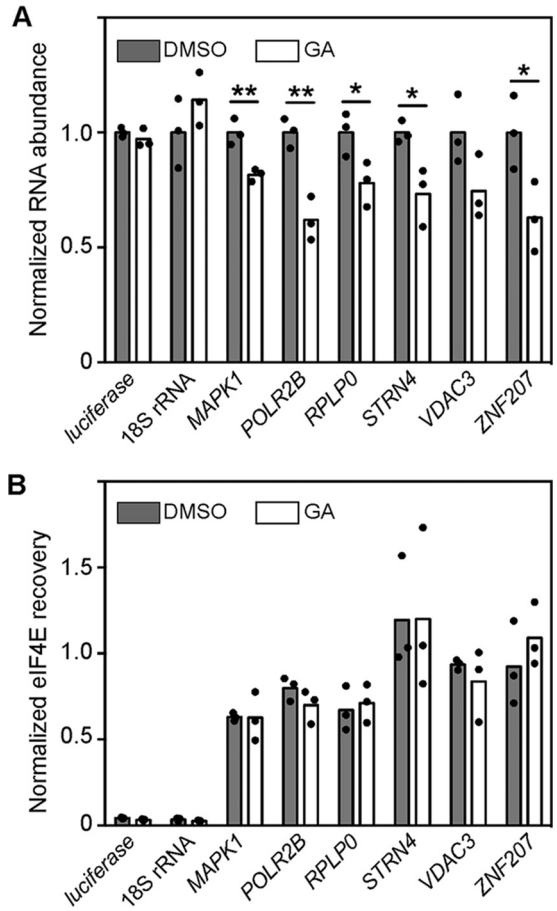

Figure 4. HSP90 inhibition causes widespread decrease in the levels of cytoplasmic capped RNAs. Triplicate cultures of U2OS-TR cells were grown for 24 h in the presence of 0.2 μM GA or DMSO vehicle control. Cytoplasmic RNA was prepared from each culture. Mixtures for each sample were prepared containing 1 μg of cytoplasmic RNA and equal amounts of uncapped luciferase RNA and capped mCherry RNA as normalization and cap-separation controls. Mixtures were split in half, with one half processed as input RNA and the other half added to recombinant eIF4E to select for capped RNAs. RNA in each input and eIF4E-recovered sample was purified and analyzed by quantitative RT-PCR for several genes, with relative abundances in each sample normalized to the mCherry control. In *A*, the normalized abundance of each input sample is presented by a *dot*, with *bars* representing mean values. In *B*, normalized eIF4E recovery was calculated as the ratio of normalized abundances in eIF4E-recovered RNA to input RNA for each gene in each biological replicate. As such, a value of 1.0 represents recovery of an RNA equivalent to that of capped mCherry RNA. Results are presented as in *A* with each *dot* indicating an individual replicate. *, $p < 0.05$; **, $p < 0.01$ by unpaired two-tailed *t* test.

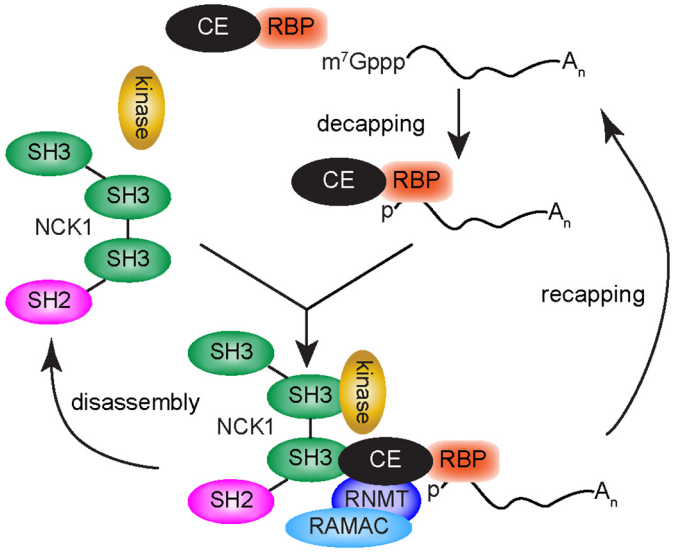

Figure 5. Proposed role for CE-binding proteins in cap homeostasis. The large number of RNA-binding proteins in the cytoplasmic CE interactome suggests a model in which recapping target RNAs are defined by binding of one or more CE-interacting proteins. In this model, the proline-rich C terminus of CE brings the CE-bound mRNP together with NCK1 and the other enzymes needed to restore the cap on uncapped mRNAs.

These analyses yielded several unanticipated findings. BioID performed by Youn *et al.* (21) identified a small number of primarily nuclear CE-interacting proteins. This was not surprising, as that study used whole-cell lysates, and nuclear CE is significantly more abundant than cytoplasmic CE. Our study used forms of CE that are restricted to the cytoplasm, and analyses were performed with cytoplasmic extracts that were essentially free of nuclear contamination. In the first approach, bio-cCE was induced to a level that approximates the endogenous protein, and cells were briefly cross-linked before lysis to stabilize native interactions (16) and minimize reassociation artifacts (35). We anticipated that this would yield a similarly small number of interacting proteins. This instead identified 45 proteins, the majority (38 proteins) of which are represented as RNA-binding proteins in the integrated human RNA-binding proteome (17). This was complemented by BioID using stable cells carrying a BirA*-cCE transgene that again was induced to a level similar to that of endogenous cytoplasmic CE. This identified 32 proteins, 23 of which were identified by Trendel *et al.* (17) as RNA-binding proteins. Eleven of the proteins identified by BioID were also among those recovered with bio-cCE (see Table S1).

Based on the results of Trotman *et al.* (12) and Mukherjee *et al.* (13), we anticipated also finding NCK1, RNMT, RAMAC, and the kinase that generates a diphosphate capping substrate from 5′-monophosphate RNA. The absence of these proteins from the cytoplasmic CE interactome was puzzling at first. However, this is true only if one considers the cytoplasmic capping complex as the major repository of cytoplasmic CE. Cytoplasmic CE is not particularly abundant, and the number of proteins identified here would reduce the possibility of identifying NCK1 and associated proteins by proteomic methods. That being said, this finding may also shed light on the question of recapping target specificity. In total, this study identified 52 RNA-binding proteins in the cytoplasmic CE interactome.

CE does not bind RNA, and results in Fig. 2*A* show that recovery of at least a few of these proteins with CE is independent of RNA. These proteins bind to the N-terminal triphosphatase domain of CE rather than the C-terminal region required for CE binding to NCK1 (Fig. 2*B*). The RNA binding specificities of many of the proteins identified here have yet to be determined, but their sheer number suggests a model (Fig. 5) in which target specificity is determined by the binding of capped or perhaps uncapped forms of a substrate RNA by one or more proteins of the CE interactome. Upon binding to CE, the mRNP joins with NCK1 for subsequent recapping. A process such as this is consistent with results of Mukherjee *et al.* (1), where the off-on cycling of 5′ caps modulates the stability of some mRNAs and the translation of others.

Given the differences in proteins recovered with bio-cCE and those identified by BioID, we were faced with classifying all of these as interacting proteins or limiting this set to the 11 that overlap between both approaches. The predominance of RNA-binding proteins in both data sets was one reason for choosing the inclusive classification, because this provides a testable hypothesis for substrate specificity. The broader classification of interacting proteins was also influenced by results of Trotman *et al.* (12), where cytoplasmic RNMT was biotinylated by BirA*-cCE, but its closely associated activating subunit (RAMAC) was not. This led us to suspect that methodological differences could in part explain differences in proteins identified here.

Finally, this study identified HSP90 as a constituent of the cytoplasmic CE interactome. As noted above, HSP90 is an ATP-dependent protein chaperone that functions in numerous signal transduction pathways (22). It is also a drug development target for cancer and other disorders (26). HSP90 inhibitors impact a number of downstream proteins; however, none of the studies to date have implicated CE, even though reduced levels of this protein lead to cell death via autophagy and apoptosis (29). Like some of the other proteins identified here, HSP90 binds the N-terminal triphosphatase domain of CE (Fig. 2*B*), and its recovery with CE is independent of RNA (Fig. 2*A*). Results with three different HSP90 inhibitors confirmed the dependence of nuclear and cytoplasmic CE on HSP90 activity. Treating cells with geldanamycin resulted in a 68% drop in bio-cCE expressed from the inducible transgene (Fig. 4*A*), a 50% loss of endogenous nuclear CE, and a 70% loss of endogenous cytoplasmic CE (Fig. 4*C*). Radicicol and geldanamycin both target the N-terminal ATP binding domain, and similar results were seen when U2OS osteosarcoma cells were treated with radicicol. Neither of these compounds is currently under evaluation as a therapeutic, but a related compound, onalespib (AT13387), is in clinical trials. Onalespib had a greater impact on the level of nuclear CE than cytoplasmic CE. Over 300 proteins have been characterized as HSP90 clients (23), but the loss of CE with HSP90 inhibitors raised the question of whether reduced cytoplasmic mRNA levels may contribute to observed losses in these proteins' abundances. The experimental results shown in Fig. 4*A* illustrate that geldanamycin treatment resulted in a statistically significant decrease in steady-state levels of six mRNAs that we have studied extensively in our work on cytoplasmic capping. Because geldanamycin treatment reduced the levels of recapping target and nontarget mRNAs, its effect on steady-state levels was most likely due to decreased nuclear capping. Although this finding needs to be expanded upon, it raises the possibility that decreases in nuclear capping and the consequent decrease in translatable mRNAs might account for the decreases observed for some proteins upon inhibition of HSP90.

Experimental procedures

Plasmid constructs

The generation of plasmid pcDNA4/TO-bio-Myc-NES-mCEΔNLS (bio-cCE; Addgene plasmid 112711) was described previously (13). A similar plasmid expressing bio-EGFP (pcDNA4/TO-bio-Myc-NES-EGFP; Addgene plasmid 112712) was created by inserting a dsDNA gBlocks gene fragment (Integrated DNA Technologies) encoding the entire bio-Myc-NES-EGFP sequence into KpnI-digested pcDNA4/TO (Thermo Fisher Scientific, V102020) using In-Fusion cloning (Clontech). Plasmid pcDNA3.1/TO-Myc-BirA*-cCE (Addgene plasmid 112713) was created by inserting two tetracycline operator sites into pcDNA3.1-Myc-BirA*-cCE (12) at the same location as in pcDNA4/TO. This was accomplished with the Change-IT site-directed mutagenesis system (Affymetrix) using 5′-phosphorylated forward primer JT93 (TGGGAGGTCTATATAAGCAGAGCTCTCCCTATCAGTGATAGAGATCTCCCTATCAGTGATAGAGATCTGGCTAACTAGAGAACCCACTG). The corresponding negative control BioID plasmid pcDNA3.1/TO-Myc-BirA*-NES (Addgene plasmid 112714) was generated from pcDNA3.1-Myc-BirA* (Addgene plasmid 35700, kindly deposited by Kyle Roux) using the Change-IT system with JT93 and 5′-phosphorylated reverse primer JT95 (CAGATATCCAGCACAGTGGCGGCCGTCATCAGGCCTCCATGGCCATATCAAGAGTAAGTCTCTCAAGCGGTGGTAGCTGAAGCTCGAGCTTCTCTGCGCTTCTCAGG), which added the HIV Rev NES downstream of BirA*.

The CE deletion constructs pcDNA3-bio-Myc-CE 2–210 (Addgene plasmid 112715) and pcDNA3-bio-Myc-CE 211–597 (Addgene plasmid 112716) were generated using the Phusion site-directed mutagenesis kit (Thermo Fisher F541) with pcDNA3-bio-Myc-CE (13) as the template. Mutagenic PCR was performed using 5′-phosphorylated primers JT164 (TGAGGGCCCTATTCTATAGTGTCACC) and JT165 (TGAGTCCTTTTTTCCATCTTCATCCTC)forpcDNA3-bio-Myc-CE2–210and5′-phosphorylated primers JT166 (GAACCAGGGTCAAGTGCATCCT) and JT167 (GGCCTCCATGGCCATAAGC) for pcDNA3-bio-Myc-CE 211–597. The sequences of all plasmids were confirmed by Sanger sequencing.

Cell culture, cell transfection, and generation of stable cell lines

All cells were grown at 37 °C under 5% CO_2 and were discarded after no more than 15 passages. U2OS-derived cell lines were grown in McCoy's 5A medium (Thermo Fisher 116600) supplemented with tetracycline-free fetal bovine serum (Atlanta Biologicals S10350) to 10% (v/v). Tetracycline-inducible U2OS (U2OS-TR) cells were described previously (10). Human embryonic kidney (HEK293) cells were cultured in Dulbecco's modified Eagle's medium (Thermo Fisher Scientific, 11995-073) supplemented with fetal bovine serum to 10% (v/v). For the experiment in Fig. 2*B*, HEK293 cells were transfected with 10 μg of pcDNA3-bio-Myc-CE 2–210 or pcDNA3-bio-Myc-CE 211–597 per 70% confluent 10-cm dish. After 24 h, cells were cross-linked, harvested, and processed as described below. For HSP90 inhibition experiments, cells were treated with the following compounds prepared in stock solutions with DMSO: geldanamycin (Cayman Chemical, 13355), radicicol (Cayman Chemical, 13089), and onalespib (Cayman Chemical, 10655).

To generate stable U2OS-TR cell lines expressing bio-EGFP or bio-cCE, U2OS-TR cells were transfected with either pcDNA4/TO-bio-Myc-NES-EGFP or pcDNA4/TO-bio-Myc-

NES-mCEΔNLS using FuGene 6 (Promega, E2691) according to the manufacturer's instructions. Cells were passaged 2 days following transfection and then maintained for 2 weeks in medium containing 400 μg/ml Zeocin (Thermo Fisher Scientific, R25001). Maintaining selective pressure with 400 μg/ml Zeocin, cells were passaged to low densities to allow formation of individual colonies that were isolated using cloning cylinders. Cell lines were expanded over several weeks in medium containing 400 μg/ml Zeocin before confirming inducible expression of bio-EGFP and bio-cCE by Western blotting and immunofluorescence. Cell harvesting and subcellular fractionation were performed as described (15).

To generate stable U2OS-TR cell lines expressing BirA* and BirA*-cCE, U2OS-TR cells were transfected with either pcDNA3.1/TO-Myc-BirA*-NES or pcDNA3.1/TO-Myc-BirA*-cCE, respectively, using FuGene 6 (Promega, E2691) according to the manufacturer's instructions. Cells were passaged 2 days following transfection and then maintained for 2 weeks in medium containing 600 μg/ml Geneticin (Thermo Fisher, 10131035). Maintaining selective pressure with 600 μg/ml Geneticin, BirA* cells were passaged to low densities to allow formation of individual colonies that were isolated using cloning cylinders. Cell lines were expanded over several weeks in medium containing 600 μg/ml Geneticin before confirming inducible expression of Myc-BirA*. Myc-BirA*-cCE cells were maintained in antibiotic as described above but were not isolated as single colonies. Inducible expression of each cell line was confirmed by Western blotting and immunofluorescence.

Immunofluorescence

Glass coverslips in the wells of a 24-well plate were each seeded with 50,000 stable cells 17 h before induction. Expression of bio-EGFP or bio-cCE was induced by the addition of tetracycline-HCl to a working concentration of 0.2 μg/ml. After 24 h, medium was removed from the coverslips, and the cells were fixed for 20 min at room temperature in PBS containing 4% formaldehyde and 0.2% (v/v) Triton X-100. Coverslips were briefly washed three times with PBS before incubating in IF Block Solution (PBS containing 1% (w/v) BSA and 0.05% (v/v) Triton X-100) for 90 min at room temperature, followed by overnight incubation at 4 °C in IF Blocking Solution containing a 1:1000 dilution of mouse anti-Myc antibody (Santa Cruz Biotechnology, Inc., sc-40). Coverslips were washed three times with IF Wash Solution (PBS containing 0.5 mM $MgCl_2$ and 0.05% (v/v) Triton X-100) at room temperature, 5 min/wash, and then incubated for 60 min in the dark at room temperature in IF Block Solution containing 0.75 μg/ml DAPI and a 1:1000 dilution of anti-mouse Alexa Fluor 594 (Thermo Fisher Scientific, A11005). After washing with IF Wash Solution as before, coverslips were mounted on glass microscope slides with ProLong Gold Antifade Mountant (Thermo Fisher P36930) and incubated overnight in the dark at room temperature to allow the mountant to cure. Images were acquired at room temperature with a Nikon Eclipse Ti-U inverted microscope fitted with a CFI Plan Apo VC 60× oil immersion objective and a Nikon DS-Qi1 monochrome digital camera. Images were analyzed using Nikon NIS-Elements AR 3.10 software. Specificity of the secondary antibody for the primary antibodies was confirmed by parallel preparation of control coverslips not treated with primary antibody.

SDS-PAGE and Western blotting

Samples in Laemmli sample buffer were heated at 95 °C for 5 min and briefly centrifuged before loading onto Mini-PROTEAN TGX gels (Bio-Rad) and electrophoresing at 150 V in Tris-glycine-SDS running buffer. Proteins were transferred to Immobilon-FL (EMD Millipore IPFL00010) polyvinylidene difluoride membranes at 100 V for 60 min at 4 °C. Membranes were blocked in Blocking Buffer (Tris-buffered saline (TBS) containing 3% (w/v) BSA) for at least 30 min at room temperature before incubating overnight at 4 °C in Blocking Buffer containing primary antibodies at the dilutions listed under "Antibodies." Membranes were washed three times in TBST (TBS plus 1% Tween 20) at room temperature, at least 10 min/wash. Secondary antibody incubations were performed for 30 min at room temperature in Blocking Buffer, with antibody dilutions listed under "Antibodies." Membranes were washed again with TBST as before and then imaged with a LI-COR Odyssey IR scanner at 700 or 800 nm as appropriate. Using LI-COR Odyssey software, band intensities were quantified following background correction. Protein abundances were then calculated following normalization with the accompanying loading control shown in each figure. GraphPad Prism version 6 software was used to plot individual data points and to perform unpaired two-tailed *t* tests, with significant results reported in each figure.

Antibodies

Primary antibodies used in this study are as follows: mouse anti-Myc (Santa Cruz Biotechnology, sc-40; 1:1000 for WB, 1:1000 for IF), rabbit anti-CE/RNGTT (Novus, NBP1-49972; 1:500 for WB), rabbit anti-FASN (Proteintech, 10624-2-AP; 1:500 for WB), rabbit anti-XPO2/CSE1L (Proteintech, 22219-1-AP; 1:1000 for WB), rabbit anti-EEF2 (One World Lab; 1:500 for WB), rabbit anti-HSP90α/β (Santa Cruz Biotechnology, sc-4947; 1:2000 for WB), rabbit anti-RUVBL1 (Proteintech, 10210-2-AP; 1:1000 for WB), rabbit anti-RUVBL2 (Proteintech, 10195-1-AP; 1:500 for WB), rabbit anti-WDR77/MEP50 (Cell Signaling, catalog no. 2823; 1:1000 for WB), mouse anti-α-tubulin (Sigma, T6199; 1:5000 for WB), rabbit anti-U2AF35 (provided by Brenton Graveley, University of Connecticut; 1:3000 for WB). Secondary antibodies used in this study are as follows: anti-mouse Alexa Fluor 594 (Thermo Fisher Scientific, A11005; 1:1000 for IF), anti-rabbit Alexa Fluor 680 (Thermo Fisher Scientific, A21109; 1:10,000 for WB), and anti-mouse Alexa Fluor 680 (Thermo Fisher Scientific, A21057; 1:10,000 for WB). Qdot 800 streptavidin conjugate (Thermo Fisher Scientific, Q10171MP; 1:10,000 for WB) was used to detect biotinylated proteins.

Cross-linking, BioID, and recovery on streptavidin beads

After a 24-h induction with 0.2 μg/ml tetracycline-HCl (Sigma, T7660), growth medium was completely removed from three or four 80–90% confluent 15-cm dishes each of bio-EGFP and bio-cCE stable cells. To each dish, 10 ml of PBS containing 0.15% formaldehyde (VWR 0493) was added and incubated at

room temperature for 10 min. To quench the cross-linking reaction, 1 ml of ice-cold PBS containing 1.25 M ice-cold glycine was added to each dish. Dishes were gently mixed by tilting and incubated for 5–10 min at room temperature. The preceding steps were all performed in a staggered, timed manner to ensure consistent treatment. Cells were then washed with PBS and harvested by scraping into PBS, pooling the bio-EGFP and bio-cCE cells into one 1.6-ml tube each. Cytoplasmic extracts were prepared as described (12, 15). For the experiment in Fig. 2*A*, $CaCl_2$ was added to cytoplasmic extracts to 5 mM, micrococcal nuclease (Thermo Fisher, 88216) was added to 0.46 units/ml (or not added as a control), and samples were incubated at room temperature for 15 min. To 1.6-ml tubes containing 15 μl (stock slurry volume) of pre-equilibrated MyOne Streptavidin T1 Dynabeads (Thermo Fisher Scientific, 65601), equal mass amounts of protein (~1000 μg/sample) were added, brought to 1 ml with YO Lysis Buffer (12), and brought to 150 mM upon the addition of 30 μl of 5 M NaCl. Tubes were incubated end-over-end for 1 h at 4 °C to bind biotinylated proteins to the beads. The beads were washed two or three times with 500 μl of ice-cold YO Lysis Buffer containing 150 mM NaCl and then two or three times with 500 μl of ice-cold 50 mM ammonium bicarbonate, incubating end-over-end at 4 °C for 10 min/wash. After removal of the final wash, beads were resuspended in either 50 mM ammonium bicarbonate (for proteomics analysis) or 2× Laemmli Sample Buffer (Bio-Rad, 1610737) containing 5% (v/v) β-mercaptoethanol (for SDS-PAGE). Samples were stored at −20 °C.

BioID, BirA*, and BirA*-cCE cells were induced with tetracycline as above and treated as described (12), except that medium was supplemented with 1 μM biotin for 14 h before lysis. Cytoplasmic extract preparation and recovery of biotinylated proteins with streptavidin beads were performed as described above.

Proteomics analysis

Protein-bound streptavidin beads were incubated in ice cold acetone at −20 °C overnight to precipitate proteins. Samples were centrifuged at 16,000 × *g* for 10 min, and supernatants were discarded. Pellets were reconstituted in 80 μl of 50 mM ammonium bicarbonate containing 0.02% ProteaseMAX surfactant (Promega, V2071) and incubated at 95 °C for 5 min. Samples were reduced with DTT at a final concentration of 5 mM at 56 °C for 20 min and alkylated with iodoacetamide (Sigma-Aldrich) at a final concentration of 16.5 mM at room temperature in the dark for 15 min. Tryptic digests were performed by adding 2 μl of 1 μg/μl trypsin supplemented with 1 μl of 1% ProteaseMAX surfactant and incubating at 37 °C for 3 h. Trypsin was inactivated upon the addition of TFA to a final concentration of 0.5%. The digestion products were centrifuged at 16,000 × *g* for 10 min, and the supernatants were collected and evaporated to dryness. Approximately 0.5 μg of peptides per sample were separated by reversed-phase ultra-performance LC on a Waters nanoACQUITY UPLC system, and mass was analyzed by a Thermo LTQ-Orbitrap Elite mass spectrometer fitted with an EASY-Spray ion source. Peptides were loaded on a Waters Symmetry C18 trap column (100 Å, 5-μm particle diameter, 180 μm × 20 mm) and desalted at a flow rate of 20 μl/min, followed by analytical separation on a second C18 reverse phase column (75-μm inner diameter × 15 cm, PepMap C18, 3 μm, 100 Å; nanoViper) at pH 2.4 using 0.1% formic acid (A1) and acetonitrile with 0.1% formic acid (B1) as mobile phases in a 90-min gradient. The heated capillary temperature and electrospray voltage on the LTQ-Orbitrap Elite were 275 °C and 1.7 kV, respectively, using top 15 data-dependent acquisition in positive ion mode.

Label-free relative quantitation

Protein identifications were obtained via the Thermo Proteome Discoverer software (version 1.4.1.14) using the Sequest search algorithm and the Uniprot Swissprot canonical *Homo sapiens* proteome (as of September 4, 2016) modified to contain our designed protein sequences. Cysteine carbamidomethylation was set as a fixed modification, whereas oxidation of methionines and deamidation of asparagines and glutamines were all set as variable modifications. Proteins were identified at a 5% false discovery rate for peptide spectral matches and 0.05 protein false discovery rate. Protein groups were filtered to include only those peptides with 99% confidence and a minimum of two peptides per protein group. The complete MS data set is available from the ProteomeXchange Consortium via the jPOST partner repository under the data set identifier PXD010368.

Measurement of RNA abundance and cap status

Triplicate cultures of U2OS-TR cells were harvested after 24-h treatment with either 0.2 μM geldanamycin or an equivalent volume of DMSO. From each culture, cytoplasmic RNA was prepared and qualified as described (12), and reduced levels of CE upon geldanamycin treatment were confirmed by Western blotting. Cap status analysis was performed by binding of cytoplasmic RNA to recombinant GST-eIF4E K119A as described (12). Briefly, for each sample, 400-μl mixtures were prepared on ice containing 1 μg of cytoplasmic RNA, 0.2 ng of 5′-triphosphate luciferase RNA (Promega, L4561), and 0.2 ng of 5′-m^7G-capped mCherry RNA (TriLink) in a buffer containing 150 mM NaCl, 0.1% (v/v) IGEPAL CA-630, 10 mM Tris, pH 7.5, 1 mM DTT, and 0.2 units/μl RNaseOUT (Thermo Fisher Scientific, 10777019). From each mixture, 200 μl was set aside to be processed as input RNA, and the other 200 μl was incubated with bead-bound GST-eIF4E K119A and washed. Input and eIF4E-recovered RNA were purified using the Direct-zol RNA MiniPrep kit (Zymo Research, R2053), eluting with 25 μl of RNase-free water. cDNA synthesis and quantitative PCR were performed as described (12), using the same primers described therein. Additional primers used were as follows: mCherry-F (ATGGTGAGCAAGGGCGAGGAG), mCherry-R (GCCACCCTTGGTCACCTTCAGC), 18S rRNA-F (CTGAGAAACGGCTACCACATC), and 18S rRNA-R (GCCTCGAAAGAGTCCTGTATTG). Using Bio-Rad CFX Manager version 3.1 software, *Cq* values were determined by regression mode, and the $\Delta\Delta Cq$ method was used to calculate relative abundances of each gene normalized to the capped mCherry spike-in control for each input and eIF4E-recovered sample. The ratio of normalized eIF4E-recovered abundance to normalized input abundance was calculated for each biological replicate as a mea-

sure of "normalized eIF4E recovery" (Fig. 4*B*). Individual data points are shown, and statistical analyses (unpaired two-tailed *t* tests) were done with GraphPad Prism version 6 software for each gene, comparing DMSO control and geldanamycin-treated samples. Results with $p < 0.05$ were considered significant.

Author contributions—J. B. T., B. A. A., and D. R. S. conceptualization; J. B. T., V. H. W., and D. R. S. resources; J. B. T., B. A. A., A. J. G., V. H. W., and D. R. S. data curation; J. B. T., B. A. A., A. J. G., and D. R. S. formal analysis; J. B. T., V. H. W., and D. R. S. supervision; J. B. T., B. A. A., V. H. W., and D. R. S. funding acquisition; J. B. T., B. A. A., A. J. G., and V. H. W. investigation; J. B. T. and D. R. S. visualization; J. B. T., B. A. A., A. J. G., and V. H. W. methodology; J. B. T., B. A. A., A. J. G., and D. R. S. writing-original draft; J. B. T., V. H. W., and D. R. S. project administration; J. B. T., B. A. A., V. H. W., and D. R. S. writing-review and editing.

References

1. Mukherjee, C., Patil, D. P., Kennedy, B. A., Bakthavachalu, B., Bundschuh, R., and Schoenberg, D. R. (2012) Identification of cytoplasmic capping targets reveals a role for cap homeostasis in translation and mRNA stability. *Cell Rep.* **2,** 674–684 CrossRef Medline
2. Kiss, D. L., Oman, K. M., Dougherty, J. A., Mukherjee, C., Bundschuh, R., and Schoenberg, D. R. (2016) Cap homeostasis is independent of poly(A) tail length. *Nucleic Acids Res.* **44,** 304–314 CrossRef Medline
3. Djebali, S., Davis, C. A., Merkel, A., Dobin, A., Lassmann, T., Mortazavi, A., Tanzer, A., Lagarde, J., Lin, W., Schlesinger, F., Xue, C., Marinov, G. K., Khatun, J., Williams, B. A., Zaleski, C., Rozowsky, J., *et al.* (2012) Landscape of transcription in human cells. *Nature* **489,** 101–108 CrossRef Medline
4. Fejes-Toth, K., Sotirova, V., Sachidanandam, R., Assaf, G., Hannon, G. J., Kapranov, P., Foissac, S., Willingham, A. T., Duttagupta, R., Dumais, E., and Gingeras, T. R. (2009) Post-transcriptional processing generates a diversity of 5′-modified long and short RNAs. *Nature* **457,** 1028–1032 CrossRef Medline
5. Kiss, D. L., Oman, K., Bundschuh, R., and Schoenberg, D. R. (2015) Uncapped 5′ ends of mRNAs targeted by cytoplasmic capping map to the vicinity of downstream CAGE tags. *FEBS Lett.* **589,** 279–284 CrossRef Medline
6. Mercer, T. R., Dinger, M. E., Bracken, C. P., Kolle, G., Szubert, J. M., Korbie, D. J., Askarian-Amiri, M. E., Gardiner, B. B., Goodall, G. J., Grimmond, S. M., and Mattick, J. S. (2010) Regulated post-transcriptional RNA cleavage diversifies the eukaryotic transcriptome. *Genome Res.* **20,** 1639–1650 CrossRef Medline
7. Mercer, T. R., Wilhelm, D., Dinger, M. E., Soldà, G., Korbie, D. J., Glazov, E. A., Truong, V., Schwenke, M., Simons, C., Matthaei, K. I., Saint, R., Koopman, P., and Mattick, J. S. (2011) Expression of distinct RNAs from 3′ untranslated regions. *Nucleic Acids Res.* **39,** 2393–2403 CrossRef Medline
8. Chen, P., Zhou, Z., Yao, X., Pang, S., Liu, M., Jiang, W., Jiang, J., and Zhang, Q. (2017) Capping enzyme mRNA-cap/RNGTT regulates hedgehog pathway activity by antagonizing protein kinase A. *Sci. Rep.* **7,** 2891 CrossRef Medline
9. Ignatochkina, A. V., Takagi, Y., Liu, Y., Nagata, K., and Ho, C. K. (2015) The messenger RNA decapping and recapping pathway in *Trypanosoma*. *Proc. Natl. Acad. Sci. U.S.A.* **112,** 6967–6972 CrossRef Medline
10. Otsuka, Y., Kedersha, N. L., and Schoenberg, D. R. (2009) Identification of a cytoplasmic complex that adds a cap onto 5′-monophosphate RNA. *Mol. Cell. Biol.* **29,** 2155–2167 CrossRef Medline
11. Thul, P. J., Åkesson, L., Wiking, M., Mahdessian, D., Geladaki, A., Ait Blal, H., Alm, T., Asplund, A., Björk, L., Breckels, L. M., Bäckström, A., Danielsson, F., Fagerberg, L., Fall, J., Gatto, L., *et al.* (2017) A subcellular map of the human proteome. *Science* **356,** eaal3321 CrossRef Medline
12. Trotman, J. B., Giltmier, A. J., Mukherjee, C., and Schoenberg, D. R. (2017) RNA guanine-7 methyltransferase catalyzes the methylation of cytoplasmically recapped RNAs. *Nucleic Acids Res.* **45,** 10726–10739 CrossRef Medline
13. Mukherjee, C., Bakthavachalu, B., and Schoenberg, D. R. (2014) The cytoplasmic capping complex assembles on adapter protein NCK1 bound to the proline-rich C-terminus of mammalian capping enzyme. *PLoS Biol.* **12,** e1001933 CrossRef Medline
14. Gonatopoulos-Pournatzis, T., Dunn, S., Bounds, R., and Cowling, V. H. (2011) RAM/Fam103a1 is required for mRNA cap methylation. *Mol. Cell* **44,** 585–596 CrossRef Medline
15. Trotman, J. B., and Schoenberg, D. R. (2018) RNA cap methyltransferase activity assay. *Bio. Protoc.* **8,** e2767 CrossRef Medline
16. Srinivasa, S., Ding, X., and Kast, J. (2015) Formaldehyde cross-linking and structural proteomics: bridging the gap. *Methods* **89,** 91–98 CrossRef Medline
17. Trendel, J., Schwarzl, T., Prakash, A., Bateman, A., Hentze, M. W., and Krijgsveld, J. (2018) The human RNA-binding proteome and its dynamics during arsenite-induced translational arrest. *bioRxiv* CrossRef
18. Baltz, A. G., Munschauer, M., Schwanhäusser, B., Vasile, A., Murakawa, Y., Schueler, M., Youngs, N., Penfold-Brown, D., Drew, K., Milek, M., Wyler, E., Bonneau, R., Selbach, M., Dieterich, C., and Landthaler, M. (2012) The mRNA-bound proteome and its global occupancy profile on protein-coding transcripts. *Mol. Cell* **46,** 674–690 CrossRef Medline
19. Castello, A., Fischer, B., Eichelbaum, K., Horos, R., Beckmann, B. M., Strein, C., Davey, N. E., Humphreys, D. T., Preiss, T., Steinmetz, L. M., Krijgsveld, J., and Hentze, M. W. (2012) Insights into RNA biology from an atlas of mammalian mRNA-binding proteins. *Cell* **149,** 1393–1406 CrossRef Medline
20. Milek, M., Imami, K., Mukherjee, N., Bortoli, F., Zinnall, U., Hazapis, O., Trahan, C., Oeffinger, M., Heyd, F., Ohler, U., Selbach, M., and Landthaler, M. (2017) DDX54 regulates transcriptome dynamics during DNA damage response. *Genome Res.* **27,** 1344–1359 CrossRef Medline
21. Youn, J. Y., Dunham, W. H., Hong, S. J., Knight, J. D. R., Bashkurov, M., Chen, G. I., Bagci, H., Rathod, B., MacLeod, G., Eng, S. W. M., Angers, S., Morris, Q., Fabian, M., Côté, J. F., and Gingras, A. C. (2018) High-density proximity mapping reveals the subcellular organization of mRNA-associated granules and bodies. *Mol. Cell* **69,** 517–532.e11 CrossRef Medline
22. Karagöz, G. E., and Rüdiger, S. G. (2015) Hsp90 interaction with clients. *Trends Biochem. Sci.* **40,** 117–125 CrossRef Medline
23. Röhl, A., Rohrberg, J., and Buchner, J. (2013) The chaperone Hsp90: changing partners for demanding clients. *Trends Biochem. Sci.* **38,** 253–262 CrossRef Medline
24. Ullrich, S. J., Moore, S. K., and Appella, E. (1989) Transcriptional and translational analysis of the murine 84- and 86-kDa heat shock proteins. *J. Biol. Chem.* **264,** 6810–6816 Medline
25. Whitesell, L., and Lindquist, S. L. (2005) HSP90 and the chaperoning of cancer. *Nat. Rev. Cancer* **5,** 761–772 CrossRef Medline
26. Zuehlke, A. D., Moses, M. A., and Neckers, L. (2018) Heat shock protein 90: its inhibition and function. *Philos. Trans. R. Soc. Lond. B. Biol. Sci.* **373,** 20160527 CrossRef Medline
27. Fang, Q., Inanc, B., Schamus, S., Wang, X. H., Wei, L., Brown, A. R., Svilar, D., Sugrue, K. F., Goellner, E. M., Zeng, X., Yates, N. A., Lan, L., Vens, C., and Sobol, R. W. (2014) HSP90 regulates DNA repair via the interaction between XRCC1 and DNA polymerase β. *Nat. Commun.* **5,** 5513 CrossRef Medline
28. Tago, K., Tsukahara, F., Naruse, M., Yoshioka, T., and Takano, K. (2004) Regulation of nuclear retention of glucocorticoid receptor by nuclear Hsp90. *Mol. Cell. Endocrinol.* **213,** 131–138 CrossRef Medline
29. Chu, C., and Shatkin, A. J. (2008) Apoptosis and autophagy induction in mammalian cells by siRNA knockdown of mRNA capping enzymes. *Mol. Cell. Biol.* **28,** 5829–5836 CrossRef Medline
30. Song, M. G., Li, Y., and Kiledjian, M. (2010) Multiple mRNA decapping enzymes in mammalian cells. *Mol. Cell* **40,** 423–432 CrossRef Medline
31. Jiao, X., Chang, J. H., Kilic, T., Tong, L., and Kiledjian, M. (2013) A mammalian pre-mRNA 5′ end capping quality control mechanism and an unexpected link of capping to pre-mRNA processing. *Mol. Cell* **50,** 104–115 CrossRef Medline
32. Aregger, M., and Cowling, V. H. (2017) Regulation of mRNA capping in the cell cycle. *RNA Biol.* **14,** 11–14 CrossRef Medline

33. Niedzwiecka, A., Marcotrigiano, J., Stepinski, J., Jankowska-Anyszka, M., Wyslouch-Cieszynska, A., Dadlez, M., Gingras, A. C., Mak, P., Darzynkiewicz, E., Sonenberg, N., Burley, S. K., and Stolarski, R. (2002) Biophysical studies of eIF4E cap-binding protein: recognition of mRNA 5′ cap structure and synthetic fragments of eIF4G and 4E-BP1 proteins. *J. Mol. Biol.* **319,** 615–635 CrossRef Medline

34. Ramanathan, A., Robb, G. B., and Chan, S. H. (2016) mRNA capping: biological functions and applications. *Nucleic Acids Res.* **44,** 7511–7526 CrossRef Medline

35. Mili, S., and Steitz, J. A. (2004) Evidence for reassociation of RNA-binding proteins after cell lysis: implications for the interpretation of immunoprecipitation analyses. *RNA* **10,** 1692–1694 CrossRef Medline

RNA-binding proteins and heat-shock protein 90 are constituents of the cytoplasmic capping enzyme interactome

Jackson B. Trotman, Bernice A. Agana, Andrew J. Giltmier, Vicki H. Wysocki and Daniel R. Schoenberg

J. Biol. Chem. 2018, 293:16596-16607.
doi: 10.1074/jbc.RA118.004973 originally published online August 30, 2018
